Mass Transfer via Femtoliter Droplets in Ping-Pong Mode

Mostafa Shojaeian and Steffen Hardt*
Institute for Nano- and Microfluidics, TU Darmstadt, 64287 Darmstadt, Germany

(Received 2 September 2019; published 9 January 2020)

Droplets with diameters in the micrometer range find numerous applications, for example, as biological reaction compartments. In that context, adding and subtracting the smallest amounts of liquid in a well-controlled manner is a key step. Here, we demonstrate a principle that allows the transfer of tiny amounts of dissolved species to an aqueous femtoliter droplet reciprocating between two aqueous reservoirs under the influence of a dc electric field. Mass transfer is size selective and adaptive, for example, via tuning the viscosity of the surrounding oil phase or the electric-field strength. We provide a map of the dynamic regimes, indicating under which conditions the reciprocating droplet motion occurs. We also formulate a model based on diffusive mass transfer that describes the amount of species taken up and transferred by the droplet. Overall, our results significantly help to facilitate the handling and manipulation of femtoliter droplets.

DOI: 10.1103/PhysRevApplied.13.014015

I. INTRODUCTION

Applications of droplet microfluidics lie in the fields of biochemical analysis [1], drug discovery and genetics [2], or synthetic biology [3], among others. Adding and extracting small amounts of liquid allow the droplets to communicate with their environment and is demonstrated to be a key step, for example, in mimicking the metabolism of synthetic cells [4,5]. Addition and extraction of small volumes to or from droplets is realized by bringing a droplet in touch with a liquid meniscus at a microchannel junction [6]; this is a process that can be supported by electric fields [7,8]. In the vast majority of droplet microfluidics research, droplets with volumes in the picoliter range or larger are considered. However, for very small droplets with volumes in the femtoliter range, some of the unit operations of droplet microfluidics become challenging [9].

Here, we demonstrate the manipulation of femtoliter droplets using electric fields. The creation or manipulation of droplets using electric fields is proven to be a versatile scheme, for example, in electrospray technology [10] or in electrowetting-based devices [11]. Our version of droplet manipulation based on dc fields utilizes the reciprocating motion of droplets between two electrodes [12–17]. In this scheme, a droplet, electrostatically attracted by an electrode, comes into contact with the electrode surface, upon which it reverses its charge and direction of motion. A natural extension is to replace the solid electrode by an aqueous medium. The key experiment in this context was conducted by Ristenpart *et al.* [18]. They pipetted an aqueous microliter droplet into an insulating liquid between a metallic pin electrode and an interface to an aqueous medium. Two different regimes are observed, depending on the parameters of the experiments (e.g., the electric-field strength): either the droplet merges with the aqueous medium, or it bounces back, similar to that found on a solid electrode.

Here, we extend the scheme of droplets reciprocating between two electrodes to femtoliter droplets, where both electrodes are liquid media. Unlike other methods for manipulating small-scale droplets, our method does not require channels of a diameter similar to that of the droplet size. We prove the controlled and selective addition and extraction of even smaller liquid volumes. Based on this, the handling of droplets with diameters as small as 2 μm becomes possible. Corresponding droplets with volumes in the femtoliter range may serve as tiny semibatch reactors, which is important in the context of synthetic cells. Alternatively, the method can be used to transfer tiny amounts of liquid in a controlled way, which represents an unconventional mode of mass transfer between two compartments.

II. MATERIALS AND EXPERIMENTAL METHODS

Experiments are performed using the microfluidic device schematically shown in Fig. 1. The key part of the chip is a cross-junction configuration. The shallow main channel is placed between two side channels of larger depth, to form a pressure barrier that prevents liquid from the side channels from protruding into the main channel.

*hardt@nmf.tu-darmstadt.de

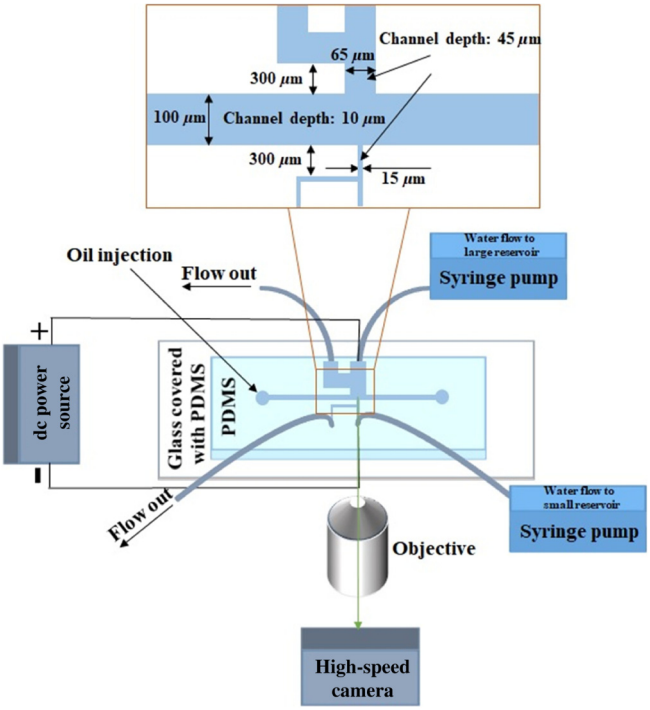

FIG. 1. Schematic of the microfluidic chip and its periphery. PDMS, polydimethylsiloxane.

The main channel contains the oil phase, and the side channels are filled with aqueous phase. The inlet sections of the side channels are connected to two ports of a power supply through needles, so that the aqueous phases filling the side channels serve as electrodes. The width of the two side channels is different, so that the electric-field lines are concentrated at the side channel of smaller width. This asymmetry enables droplet production through electric-field pulses from the side channel of smaller width.

The microfluidic chip is fabricated using the soft lithography protocol. In brief, an SU-8 photoresist on a silicon wafer is microstructured using UV lithography. The resulting structure serves as a mold for creating the chip. The polydimethylsiloxane (PDMS)-cross-linker mix, purchased from Dow Corning (Sylgard 184 Silicone Elastomer), is degassed in a desiccator, after which it is cast onto the mold to form the structures of the microfluidic chip. For this purpose, a PDMS-to-cross-linker ratio of 10:1 is used, followed by curing at 75 °C for 40 min. To create the PDMS cover of the chip, a PDMS-to-cross-linker mixture of 20:1 is spin-coated on a glass slide at 2000 rpm for 30 s, followed by a curing process over about 15 min at 75 °C. After punching the inlet and outlet holes, the chip substrate is gently placed onto a glass slide covered with the thin PDMS layer. Finally, the arrangement is cured overnight, leading to PDMS-PDMS bonding.

During the experiments, the oil phase is filled into the main channel using capillary suction, i.e., the oil spontaneously fills the channel, since it wets the channel walls very well. By contrast, since PDMS is hydrophobic, aqueous liquids are introduced into the side channels via syringe pumps (KD Scientific Inc.) The pumps are kept running to build up a pressure head to fix the oil-aqueous interfaces at their desired positions. A high-voltage sequencer (LabSmith HVS448) is employed as a power supply to provide pulsed and dc voltages. A high-speed camera (Redlake Motion Pro Series Y) is mounted on an inverted microscope (Nikon Eclipse Ti) to capture the behavior and motion of droplets. Fluorescence microscopy is utilized to visualize droplets containing rhodamine B. The same inverted microscope with a 50× objective (numerical aperture 0.8) is used to capture images of the fluorescent droplets in epifluorescence mode. An epifluorescence illuminator (Nikon Intensilight C-HGFI) is used for fluorescence excitation. An Andor iXion EM+ DU-897 EMCCD camera with 50-ms exposure time captures the emitted signals, and the NIS-elements software is employed for image acquisition. To infer the dye concentration inside the droplets, a relationship between fluorescence intensity and concentration is needed. For this purpose, droplets are produced from a reservoir with a known dye concentration and their fluorescence intensity is measured. To determine the concentration inside the droplets studied in the mass-transfer experiments, a linear relationship between fluorescence intensity and concentration is assumed.

The working fluids in our experiments are water as the aqueous phase at different salinities, through the addition of NaCl, and standard silicone oils with kinematic viscosities of 500, 1000, 2000, and 5500 mm^2/s. Additionally, 1000 mm^2/s silicone oil AP is used, which is a modified version of standard silicone oils with added phenyl groups. The silicone oils are purchased from Sigma Aldrich, Dow Corning, or HUDY.

III. REGIMES OF DROPLET MOTION

Figure 2(a) shows the key feature of the microfluidic design, i.e., the channel junction. Droplets performing the reciprocating motion between the two oil-aqueous interfaces are produced by applying a voltage pulse between the electrodes. The electrohydrodynamic generation of droplets we are utilizing here has been described before in Refs. [19–21]. To unambiguously assign the liquid interface at which the droplets are generated, the side channels differ in widths. Via the concentration of electric-field lines, the liquid interface at the small reservoir experiences a higher electric-field strength than that at the other one, which guarantees that the droplets are produced from the small reservoir. In Fig. 2(a), a droplet produced that way (diameter approximately 8 μm) is visible at the center of the main channel. Details related to droplet production in our microfluidic device can be found in Appendixes A

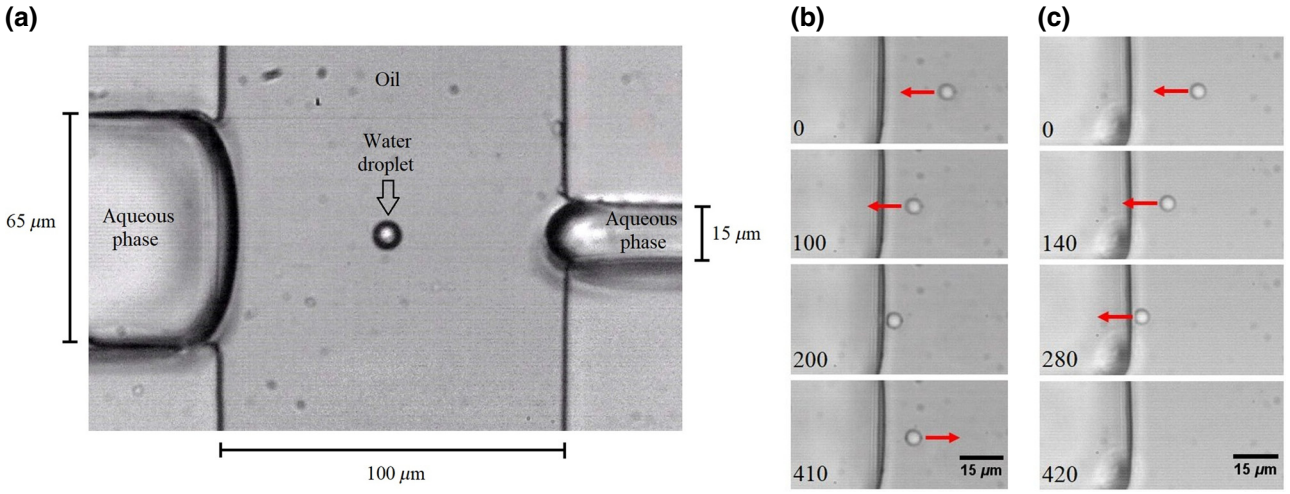

FIG. 2. Microchannel junction and modes of droplet motion. (a) Microchannel junction with two side branches filled with aqueous solutions. The main channel is filled with oil. The aqueous droplet is produced at the right oil-water interface by applying a short electric-field pulse. (b) When the voltage between the two oil-water interfaces exceeds a threshold value, a droplet only briefly touches the liquid interface, after which it reverses its direction of motion. The instantaneous direction of motion is indicated by the arrows. (c) Below the threshold voltage, a droplet coalesces with the aqueous reservoir. The numbers given in the individual frames in (b),(c) denote the time in milliseconds.

and B. In the following, the left-side channel in Fig. 2(a) will be denoted "large reservoir" whereas the right-side channel is the "small reservoir."

When a dc voltage is switched on between the electrodes, under suitable conditions, a reciprocating motion of droplets (in the following referred to as ping-pong mode) sets in between the liquid interfaces (see Video 1 within the Supplemental Material [22]). Time-lapse images of such a droplet at the large reservoir are shown in Fig. 2(b), where the arrows denote the direction of motion. The droplet has a diameter of approximately 6 μm, a voltage of 300 V is applied, and the main channel is filled with 2000 mm^2/s silicone oil. When reaching the oil-aqueous interface, the droplet does not merge with the aqueous reservoir, but bounces back. The noncoalescence of oppositely charged microliter droplets was studied by Ristenpart *et al.* [18]. They showed that a droplet bounced off from a liquid interface for sufficiently high values of the electric-field strength and oil viscosity. This behavior can be explained by considering the geometric shape of the liquid bridge forming between the droplet and the liquid interface. The liquid bridge is a result of two Taylor cones forming at the droplet surface and at the liquid interface. The two principal curvatures of the oil-aqueous interface have opposite signs at the neck of the bridge. With increasing electric-field strength, the concave curvature reduces, such that the Laplace pressure inside the bridge increases, leading to a rapid breakup of the liquid bridge. Corresponding to these predictions, when the voltage is reduced to 200 V, the droplet merges with the large reservoir [cf. Fig. 2(c)]. After its initial discovery, the noncoalescence of droplets driven by electric fields has been studied in more detail. Among others, predictions for the critical cone angle separating the coalescence from the bouncing regime were made [23,24]. In our experiments, the droplets are orders of magnitude smaller than those studied in the original noncoalescence experiments [18], which means that the Taylor cones and liquid bridges have submicron dimensions. This makes it impossible to study the formation and dynamics of these structures based on available experimental methods. Nevertheless, experiments performed at 10 000 frames/s, which is the limiting frame rate under the given illumination conditions, indicate that the liquid bridge exists only for a time span of less than 0.1 ms. For convenience, most of the experiments reported here are performed on droplets with diameters of about 9 μm for 1000 mm^2/s silicone oil AP and 6 μm for standard silicone oils. However, we observe the same behavior with droplets as small as 2 μm.

The frequency of the reciprocating droplet motion can be tuned by varying the applied voltage and the oil viscosity. The influence of these two parameters is shown in Fig. 3(a), where the frequency, f, of droplet motion is displayed as a function of the oil viscosity, η. The two lines represent fits of the form $f \propto \eta^{-1}$, which is the prediction of the Hadamard–Rybczynski equation [25] in the limiting case that the viscosity of the continuous phase is much larger than that of the droplet viscosity. An assumption inherent in the model equation is that the droplet charge does not change with the oil viscosity. As it is apparent from Fig. 3(a), the experimental data are roughly consistent with the model equation. This indicates that, although the droplet motion is significantly slowed down at higher oil viscosities, the charge transferred from the reservoir to

the droplet remains largely unaffected. It becomes apparent that the oil viscosity has a large influence on the droplet frequency.

As mentioned above, the ping-pong mode occurs only in a specific parameter range. For potential applications of the principle, we report here that it will be important to identify the different physical regimes of electrically driven droplets between two liquid interfaces. We identify three different regimes. Apart from the bouncing regime (corresponding to the ping-pong mode), there is a coalescence regime and a failure regime. The coalescence regime is the regime in which a droplet merges with the liquid filling the side channels. In the failure regime, the Maxwell stress acting on the liquid interface becomes so large that the aqueous phase permanently protrudes into the oil phase, i.e., the capillary-pressure barrier breaks down. In the experiments reported here, this occurs at the side channel with smaller width (see Appendix C for more details).

Figures 3(b) and 3(c) provide maps of these three regimes, in terms of the applied voltage, the viscosity of the oil phase, and the salt concentration in the aqueous phase. The choice of these parameters is motivated by previous work [18,23,24], which gives clear indications that the electric-field strength and salt concentration are key parameters and suggests that the properties of the continuous phase also have an influence. Each square symbol indicates a parameter combination for which experiments are performed. The black squares mark the coalescence regime. The colored areas approximately indicate the different regimes. In Fig. 3(b), the salt concentration is kept fixed at 1 M NaCl, while different silicone oils are used. In Fig. 3(c), 1000 mm^2/s silicone oil AP is used, while the salt concentration is varied. Because of the excellent reproducibility of droplet production in silicone oil AP (cf. Appendix B), this type of oil (only available with viscosities of 100 and 1000 mm^2/s) is used whenever possible. Figures 3(b) and 3(c) clearly highlight the influence of the voltage. A voltage that is too low results in coalescence, whereas a voltage that is too high leads to failure. The existence of a lower boundary of the coalescence regime, in terms of voltage, is related to the fact that the electric-field strength determines the characteristic angle of the cones from which the liquid bridge is formed [18,23,24]. For field strength values that are too low, the convex curvature of the liquid bridge becomes too high, which prevents the breakup of the bridge driven by the Laplace pressure. With increasing viscosity of the oil phase, the voltage range where bouncing is observed becomes broader, extending to lower voltages. This is consistent with recent observations on the coalescence of oppositely charged drops in liquids with different viscosities [26], and thus, indicates that increasing the viscosity of the oil phase decreases the chance of coalescence. Reducing the salt concentration shifts the voltage interval in which bouncing is observed to higher values or, in other words, can bring the system from the bouncing to the coalescence regime at fixed voltage. Similar effects of salt concentration are observed for much larger droplets [18]. Reducing the salt concentration also increases the voltage related to failure. The dependence of the interfacial tension on salt concentration offers a possible explanation in this context. It has been shown that, in combination with small amounts of ionic surfactants, NaCl significantly reduces the interfacial tension

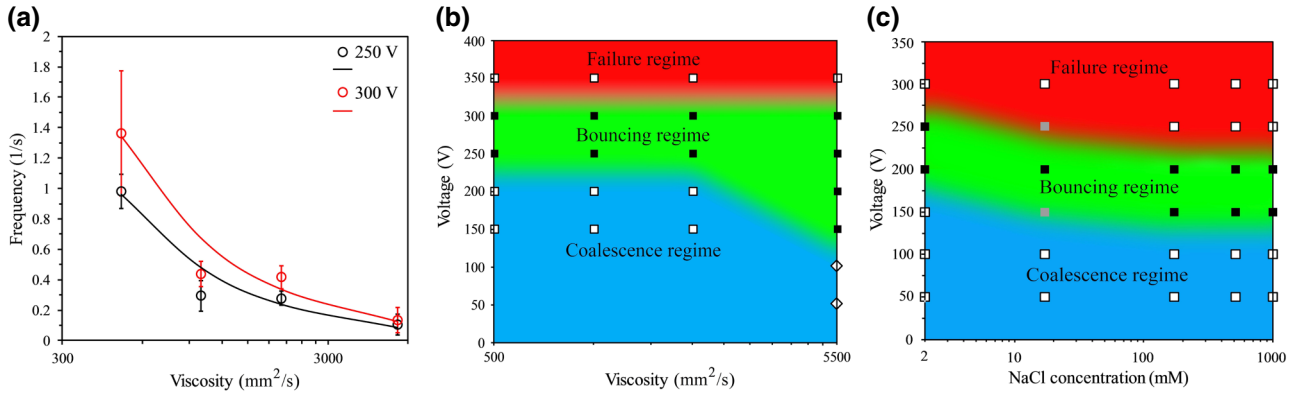

FIG. 3. Characterization of reciprocating droplet motion. (a) Frequency of reciprocating motion as a function of oil viscosity for two different voltages. The symbols mark experimental data as the average of six measurements for each viscosity, with the errors bars representing the standard deviation. The curves are fits according to the prediction of the Hadamard–Rybczynski equation. (b) Dynamic regimes corresponding to the setup shown in Fig. 2(a) in a space spanned by viscosity and voltage. The filled symbols represent the bouncing regime, the underlying colors indicate the boundaries between the different regimes. The open square symbols are data points that either belong to the coalescence or to the failure regime. The diamond-shaped symbols represent a special situation where a droplet stays at the liquid interface after touching it, but does not merge with the aqueous reservoir. (c) The same as that in (b), but in a space spanned by NaCl concentration and voltage. The gray symbols represent data points that could not be unambiguously assigned to one of the regimes.

between silicone oil and water [27]. This can be explained by considering the Debye layer thickness around charged surfactant molecules. The addition of NaCl reduces the Debye layer thickness and, therefore, the repulsive force between neighboring surfactant molecules, thereby allowing more molecules to adsorb at the silicone oil-water interface. Small amounts of surface-active species often cannot be excluded from experiments. As a result, the addition of NaCl will reduce the capillary-pressure barrier and promote the protrusion of aqueous phase from the side channels into the main channel, when a voltage is applied.

The boundaries between the different regimes are partially characteristic for the specific setup used in the experiment. Naturally, it is not the voltage but the local electric-field strength at the liquid interfaces that governs the physics. Also, at which values of the local electric-field strength the transition from bouncing to failure will occur depends on a number of parameters, such as the pressure head used to introduce the aqueous phase into the side channels or the liquid-liquid contact angle at the channel walls. The intention behind Figs. 3(b) and 3(c), however, is to map different regimes in a qualitative manner and to highlight the limiting factors for the ping-pong mode.

IV. MASS TRANSFER TO DROPLETS

One main objective of the work reported here is to study mass transfer from the aqueous phase filling the side channels to a droplet reciprocating between the two liquid interfaces. In an application context, mass transfer could enable (bio)chemical reactions in a tiny reaction space in semibatch mode, with educts being supplied to a droplet and products extracted from it. Alternatively, the setup shown in Fig. 2(a) could be used to transfer tiny amounts of liquid between two reservoirs.

We study both the transfer of dissolved molecular species and nanoparticles. Figure 4 shows three selected snapshots of experiments conducted with fluorescent polystyrene beads of 500 nm in diameter. The individual frames in Fig. 4 are obtained by superposing image sections recorded with a fluorescence microscope on brightfield images. Figure 4(a) shows the small reservoir filled with a nanoparticle suspension. A droplet containing nanoparticles is created by applying a voltage pulse. The droplet (diameter approximately 12 μm) is shown in Fig. 4(b) close to the liquid interface at the large reservoir. Remarkably, when such a droplet undergoes reciprocating motion between the two liquid interfaces, no nanoparticles are transferred between the droplet and the aqueous reservoirs. Apparently, the throat of the liquid bridge is too narrow and/or exists for a too short a time span to let 500 nm particles pass. To transfer nanoparticles from the small to the large reservoir, it is necessary to switch from the bouncing regime to the coalescence regime by reducing the voltage. Figures 4(b) and 4(c) show two subsequent images from the video recording, immediately before and after the coalescence event. The time increment between the images is 14 ms. Within this time span, the droplet merges with the aqueous reservoir. The nanoparticles are distributed over the liquid interface, as shown in Fig. 4(c).

When transferring a molecular dye dissolved in one of the aqueous reservoirs, a different scenario emerges. Experiments are performed with rhodamine B, which is a fluorescent dye that can be considered as uncharged [28,29]. The liquid inside the large reservoir contains the dye, while the liquid inside the small reservoir is water with 1 M NaCl. A droplet in ping-pong mode, initially containing no dye, starts to fluoresce after coming into contact with the large reservoir. The droplet picks up dye at the large reservoir and releases it at the small reservoir. The fluorescence increases during the first few cycles, after which time it takes a more or less constant value. This shows that mass transfer via femtoliter droplets in ping-pong mode is selective: dissolved molecules are transferred, while 500 nm particles are rejected. The dye concentration inside the droplet as a function of cycle number is shown in Fig. 5 for two different values of oil viscosity. The two different data sets in each panel represent the intensity inside the droplet after touching the interface at the large and small reservoir, respectively. The constant values reached after a few cycles represent a dynamic equilibrium state: the amount of dye taken up at the large reservoir equals the amount released at the small reservoir.

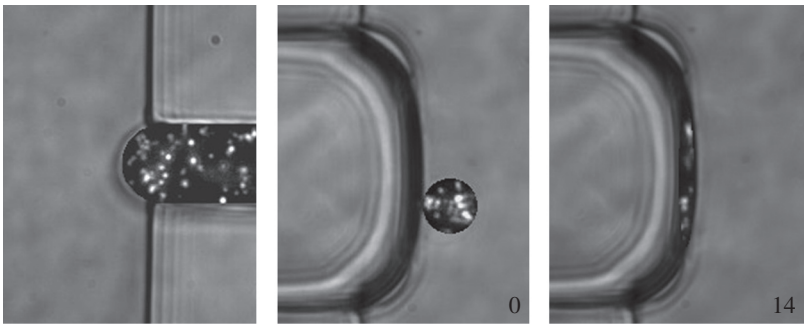

FIG. 4. Transfer of 500 nm particles between two aqueous reservoirs. (a) Small reservoir filled with a suspension of 500 nm particles. (b) Particle-laden droplet at the oil-aqueous interface of the large reservoir immediately before coalescence. (c) Oil-aqueous interface immediately after coalescence with the droplet. Nanoparticles are distributed over the interface. The numbers given in the individual frames in (b),(c) denote the relative time in milliseconds.

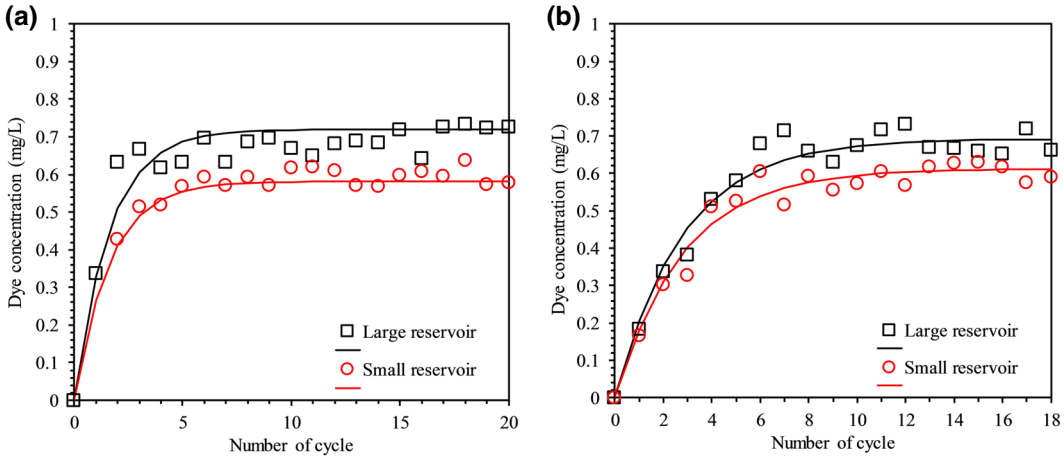

FIG. 5. Dye concentration inside a droplet as a function of cycle number, when transferring rhodamine B from the large to the small reservoir. (a) Data for 500 mm^2/s silicone oil filling the main channel. Dye concentrations after touching the large and small reservoirs are shown. The symbols represent experimental data; the curves are fits based on Eq. (1). (b) The same as that in (a), but with 1000 mm^2/s silicone oil filling the main channel.

V. MASS-TRANSFER MODEL

To model the mass-transfer process, we make use of the fact that, for rhodamine B, electrophoretic transport is negligible and set up a model for purely diffusive mass transfer via

$$N_t = kA\Delta t\Delta c, \tag{1}$$

where N_t is the number of moles transferred when a droplet touches a reservoir, k is a mass-transfer coefficient, A is a characteristic cross-section area of the liquid bridge forming between the droplet and the reservoir, Δt is a characteristic opening time of the liquid bridge, and Δc is the difference in molar concentration between a droplet and a reservoir. k, A, and Δt are not directly measurable, so we combine them into a dimensionless fit parameter, $\alpha = kA\Delta t/V_d$, where V_d is the droplet volume. Since the conditions at the large and small reservoirs are different (especially in terms of the curvature of the interface), we allow two different fit parameters, α_l and α_s, representing mass transfer at the large and small reservoir, respectively.

Species transfer occurs via the thin liquid bridge forming between the droplet and a reservoir. As indicated above, electrophoretic transport of rhodamine B is negligible. Potentially, apart from diffusive transport, advective transport could come into play. The latter is very difficult to study experimentally, since the liquid neck has submicron dimensions. In the present case, our goal is to study mass transfer in the simplest possible scenario. Therefore, we hypothesize that advective transport can be neglected. Referring to Eq. (1), for the large reservoir $\Delta c = c_l - c_{d,l}$, and for the small reservoir $\Delta c = c_{d,s} - c_s$, wherein $c_{d,l}$ and $c_{d,s}$ denote the species concentrations inside the droplet when in contact with the large and small reservoirs, respectively; and c_l and c_s are the concentrations inside the large and small reservoirs, respectively. The large reservoir has a fixed concentration, that is, c_l, whereas initially the concentration vanishes inside the small reservoir. Initially, the droplet (generated from the small reservoir) does not contain dissolved species. Notably, $kA\Delta t$ has units of m^3, and therefore, α is a dimensionless parameter that has to be less than unity. The concentration inside the reciprocating droplet after touching the large reservoir $(N+1)$ times is given by

$$c_{d,l}^{(N+1)} = c_{d,s}^{(N)} + \alpha_l[c_l - c_{d,s}^{(N)}], \tag{2}$$

where the superscript refers to the cycle number. Likewise, the concentration inside the droplet after touching the small reservoir $(N+1)$ times is given by

$$c_{d,s}^{(N+1)} = c_{d,l}^{(N+1)} - \alpha_s[c_{d,l}^{(N+1)} - c_s]. \tag{3}$$

Since initially $c_s = 0$ and the volume of the small reservoir is much larger than that of the droplet volume, we can safely assume that c_s stays very small during the whole process. Species that are deposited close to the oil-aqueous interface of the small reservoir will spread over the reservoir by diffusion. Therefore, in the following, we assume $c_s = 0$. Accordingly, Eqs. (2) and (3) can be reformulated as recursion relations

$$c_{d,l}^{(N+1)} = (1 - \alpha_l - \alpha_s + \alpha_l\alpha_s)c_{d,l}^{(N)} + \alpha_l c_l \tag{4}$$

and

$$c_{d,s}^{(N+1)} = (1 - \alpha_l - \alpha_s + \alpha_l\alpha_s)c_{d,s}^{(N)} + (\alpha_l - \alpha_l\alpha_s)c_l. \tag{5}$$

These relations have explicit solutions of the forms

$$c_{d,l}^{(N)} = b_l \sum_{i=1}^{N} a_l^{i-1} \tag{6}$$

$$c_{d,s}^{(N)} = b_s \sum_{i=1}^{N} a_s^{i-1}, \tag{7}$$

where

$$\begin{aligned} a &= a_l = a_s = 1 - \alpha_l - \alpha_s + \alpha_l\alpha_s \\ b_l &= \alpha_l c_l \\ b_s &= (\alpha_l - \alpha_l\alpha_s)c_l \end{aligned} . \tag{8}$$

Closed-form expressions of the concentrations can be obtained by recognizing that Eqs. (6) and (7) have the form of a geometric series:

$$c_{d,l}^{(N)} = \frac{\alpha_l[(1 - \alpha_l - \alpha_s + \alpha_l\alpha_s)^N - 1]}{-\alpha_l - \alpha_s + \alpha_l\alpha_s} c_l \tag{9}$$

$$c_{d,s}^{(N)} = \frac{[\alpha_l - \alpha_l\alpha_s][(1 - \alpha_l - \alpha_s + \alpha_l\alpha_s)^N - 1]}{-\alpha_l - \alpha_s + \alpha_l\alpha_s} c_l. \tag{10}$$

The asymptotic values of these expressions for $N \to \infty$ are given by

$$c_{d,l}^{(\infty)} = \frac{-b_l}{a - 1} \tag{11}$$

$$c_{d,s}^{(\infty)} = \frac{-b_s}{a - 1}, \tag{12}$$

providing that $|a| < 1$. Notably, in this asymptotic limit, a droplet still takes up dissolved species at the large reservoir and releases species at the small reservoir. However, the concentration inside the droplet no longer changes, since the amount of species taken up is equal to the amount released.

Equations (9) and (10) are used for modeling the experimental data obtained with rhodamine B. For this purpose, a Gaussian least-squares method is used to determine α_l and α_s. The solutions are computed using the generalized reduced gradient (GRG) solver, which is a steepest descent method for solving nonlinear equations with constraints. It is ensured that the solutions are independent of the initial guess for the solution. The curves shown in Figs. 5(a) and 5(b) represent the corresponding model fits. The resulting parameter values are $\alpha_l = 0.331$ and $\alpha_s = 0.192$ for Fig. 5(a) and $\alpha_l = 0.207$ and $\alpha_s = 0.116$ for Fig. 5(b). Increasing the oil viscosity, therefore, reduces the mass-transfer coefficients. We hypothesize that an increase in viscosity reduces the cross-section area and/or the opening time of the liquid bridge between the droplet and the reservoir. Overall, the experimental data follow the trend predicted by the model, which suggests that the model captures the essential mass-transfer mechanism.

VI. CONCLUSIONS

We study the reciprocating motion of femtoliter droplets between two aqueous reservoirs under dc electric fields. The regimes in which this so-called ping-pong motion occurs are identified in terms of the voltage, salt concentration, and viscosity of the surrounding oil phase. Most importantly, we study mass transfer between the two reservoirs and the droplet. While 500 nm polystyrene beads cannot be transferred from the reservoirs to a reciprocating droplet, the transfer of a fluorescent dye is proven. In this context, it is shown that a model based on diffusive mass transfer is able to describe the experimental data. Corresponding droplets with volumes in the femtoliter range may serve as tiny semibatch reactors, allowing the addition of reagents and extraction of products. Alternatively, the method can be used to transfer tiny amounts of liquid between two reservoirs in a selective and controllable way.

ACKNOWLEDGMENTS

We kindly acknowledge support from the LOEWE CompuGene Project, funded by the Hessian Ministry of Science and Art.

APPENDIX A: TIME-LAPSE IMAGES OF DROPLET GENERATION

Figure 6 displays time-lapse images showing the generation of a water droplet (containing 1 M NaCl) using a voltage pulse. The droplet is generated in 1000 mm^2/s silicone oil AP by application of a voltage pulse of 400 V with a duration of 10 ms. It can be seen that the oil-water interface starts to deform upon triggering the voltage pulse. At the end of the pulse, the electrified liquid jet reaches its maximum length and, due to the Maxwell stress exceeding the capillary pressure at the tip, a droplet pinches off. This is followed by retraction of the jet. The fact that the droplet is created from the small reservoir can be qualitatively explained by the converging electric-field lines and scaling of the Maxwell stress ($\sim E^2$). The droplet size can be tuned by varying the voltage pulse and amplitude, where the salt concentration and viscosity of the aqueous phase can play a significant role [21].

APPENDIX B: SIZE DISTRIBUTION OF THE PRODUCED DROPLETS

The size distribution of the droplets produced as described in Appendix A is shown in Fig. 7. The distribution corresponds to the results obtained for 24 individual droplets produced in 1000 mm^2/s silicone oil AP, applying a voltage amplitude of 400 V over 10 ms. If desired, the size distribution can be narrowed down by carefully tuning the electric and fluidic parameters. However, in the current study, this is of secondary importance. Referring to

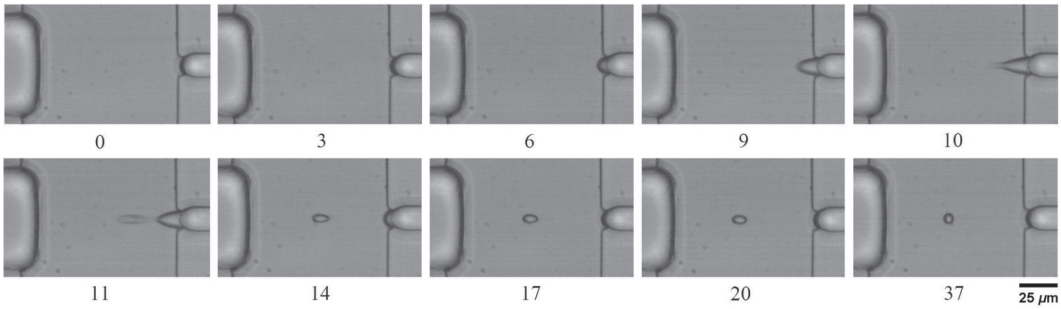

FIG. 6. Time-lapse images of the on-demand production of a water droplet using a voltage of 400 V and a pulse duration of 10 ms. The numbers below the individual frames denote the time in milliseconds.

Fig. 7, the average droplet diameter is about 8.7 μm with a standard deviation of 1.5 μm.

The type of silicone oil has an influence on the droplet size distribution and the reproducibility of droplet production. AP silicone oils have phenyl groups attached to the polymer chains. They are reported to show a higher threshold, with respect to dielectric breakdown, compared with that of standard silicone oils [30], probably because the generation and/or migration of charges is more efficiently suppressed. We find that using AP silicone oils is important to render droplet generation reproducible. In this case, droplet generation can always be achieved with the same parameters (in terms of voltage amplitude and pulse duration). However, when using standard silicone oils instead, memory effects are observed, i.e., the parameters needed to produce droplets are different for the first droplet relative to subsequent ones. Therefore, droplets produced in standard silicone oils require some readjustment of the electric parameters. The corresponding droplets tend to be smaller than those produced in silicone oil AP, but, because of the reproducibility issues mentioned above, we refrain from displaying their size distribution.

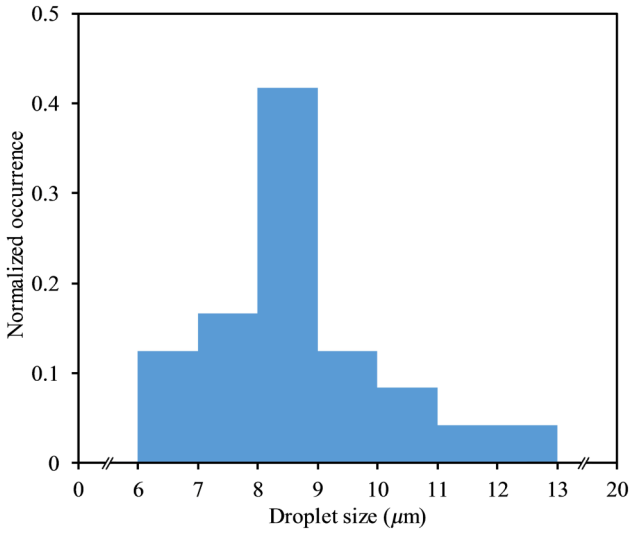

FIG. 7. Size distribution of water droplets in 1000 mm^2/s silicone oil AP, using a pulse amplitude of 400 V and a pulse duration of 10 ms.

APPENDIX C: TIME-LAPSE IMAGES OF FAILURE

Figure 8 shows time-lapse images of the electric-field-induced failure of the capillary barrier at the small reservoir. The experiment is performed with 1000 mm^2/s silicone oil AP and water containing 1 M NaCl, applying a voltage amplitude of 300 V. It can be seen that at the small reservoir the aqueous phase protrudes into the oil phase. Finally, a short circuit occurs at the large reservoir, resulting in the formation of a multitude of droplets.

The breakdown of the capillary barrier is a result of the Maxwell stress at the liquid interface exceeding the maximum Laplace pressure. To obtain a qualitative understanding of this process, for simplicity, we neglect the back pressure that needs to be applied to keep the two reservoirs filled with water. In an order-of-magnitude sense, the maximum Laplace pressure that can be generated at the junction between the main channel and a side channel is given by $\Delta p_L \sim \gamma(w^{-1} + h^{-1})$, where w is the width of the side channel and h is the depth of the main channel. Since, in the present case, $h = 10$ μm, while $w = 65$ μm and $w = 15$ μm for the large and small reservoirs, respectively, the Laplace pressure is dominated by the depth of the main channel. As a result, there is no large difference between the maximum Laplace pressures at the interfaces between the main channel and the two side channels. In terms of the Maxwell stress, however, there is a large difference between the two interfaces. The aqueous NaCl solution can be viewed as a conductor, which means that both the interface between aqueous solution and oil and the interface between aqueous solution and the wall material are isopotential surfaces. As a result, the electric-field lines converge between the large and small reservoirs, resulting in a higher electric-field strength at the oil-aqueous interface of the small reservoir. When converting the field strength to a stress, this disparity between the large and

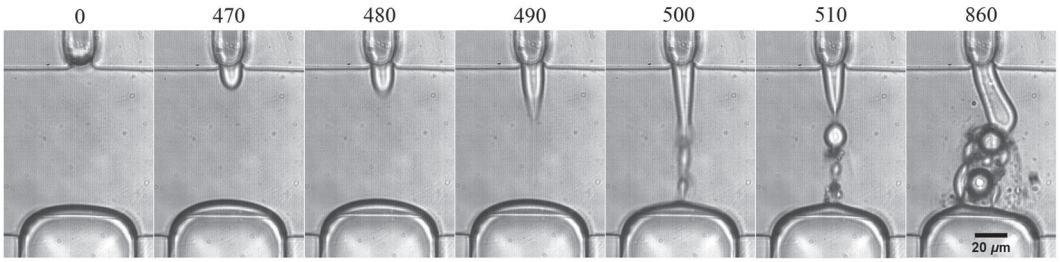

FIG. 8. Time-lapse images of the failure of the capillary barrier at the small reservoir. A constant voltage of 300 V is applied. The numbers above the individual frames denote the time in milliseconds.

small reservoirs is amplified, owing to the scaling of the Maxwell stress by E^2. Therefore, we expect the failure to occur at the small reservoir, which is confirmed by the results shown in Fig. 8.

[1] E. Y. u. Basova and F. Foret, Droplet microfluidics in (bio)chemical analysis, Analyst **140**, 22 (2015).

[2] P. C. Gach, K. Iwai, P. W. Kim, N. J. Hillson, and A. K. Singh, Droplet microfluidics for synthetic biology, Lab Chip **17**, 3388 (2017).

[3] N. Shembekar, C. Chaipan, R. Utharala, and C. A. Merten, Droplet-based microfluidics in drug discovery, transcriptomics and high-throughput molecular genetics, Lab Chip **16**, 1314 (2016).

[4] M. Weiss, J. P. Frohnmayer, L. T. Benk, B. Haller, J.-W. Janiesch, T. Heitkamp, M. Börsch, R. B. Lira, R. Dimova, R. Lipowsky, E. Bodenschatz, J.-C. Baret, T. Vidakovic-Koch, K. Sundmacher, I. Platzman, and J. P. Spatz, Sequential bottom-up assembly of mechanically stabilized synthetic cells by microfluidics, Nat. Mater. **17**, 89 (2018).

[5] T. Beneyton, D. Krafft, C. Bednarz, C. Kleineberg, C. Woelfer, I. Ivanov, T. Vidaković-Koch, K. Sundmacher, and J. C. Baret, Out-of-equilibrium microcompartments for the bottom-up integration of metabolic functions, Nat. Commun. **9**, 2391 (2018).

[6] H. Song, H. Li, M. S. Munson, T. G. Van Ha, and R. F. Ismagilov, On-chip titration of an anticoagulant argatroban and determination of the clotting time within whole blood or plasma using a plug-based microfluidic system, Anal. Chem. **78**, 4839 (2006).

[7] A. R. Abate, T. Hung, P. Mary, J. J. Agresti, and D. A. Weitz, High-throughput injection with microfluidics using picoinjectors, Proc. Natl. Acad. Sci. **107**, 19163 (2010).

[8] S. Zeng, X. Pan, Q. Zhang, B. Lin, and J. Qin, Electrical control of individual droplet breaking and droplet contents extraction, Anal. Chem. **83**, 2083 (2011).

[9] M. Leman, F. Abouakil, A. D. Griffiths, and P. Tabeling, Droplet-based microfluidics at the femtolitre scale, Lab Chip **15**, 753 (2015).

[10] P. Kebarle and U. H. Verkerk, Electrospray: From ions in solution to ions in the gas phase, what we know now, Mass Spectrom. Rev. **28**, 898 (2009).

[11] F. Mugele and J. Baret, Electrowetting: From basics to applications, J. Phys. Condens. Matter **17**, R705 (2005).

[12] S. H. Yang and D. J. Im, Electrostatic origins of the positive and negative charging difference in the contact charge electrophoresis of a water droplet, Langmuir **33**, 13740 (2017).

[13] M. Hase, S. N. Watanabe, and K. Yoshikawa, Rhythmic motion of a droplet under a dc electric field, Phys. Rev. E **74**, 3 (2006).

[14] T. Kurimura, M. Ichikawa, M. Takinoue, and K. Yoshikawa, Back-and-forth micromotion of aqueous droplets in a dc electric field, Phys. Rev. E **88**, 1 (2013).

[15] J. G. Kim, D. J. Im, Y. M. Jung, and I. S. Kang, Deformation and motion of a charged conducting drop in a dielectric liquid under a nonuniform electric field, J. Colloid Interface Sci. **310**, 599 (2007).

[16] D. J. Im, M. M. Ahn, B. S. Yoo, D. Moon, D. W. Lee, and I. S. Kang, Discrete electrostatic charge transfer by the electrophoresis of a charged droplet in a dielectric liquid, Langmuir **28**, 11656 (2012).

[17] D. J. Im, J. Noh, D. Moon, and I. S. Kang, Electrophoresis of a charged droplet in a dielectric liquid for droplet actuation, Anal. Chem. **83**, 5168 (2011).

[18] W. D. Ristenpart, J. C. Bird, A. Belmonte, F. Dollar, and H. A. Stone, Non-coalescence of oppositely charged drops, Nature **461**, 377 (2009).

[19] M. He, J. S. Kuo, and D. T. Chiu, Electro-generation of single femtoliter- and picoliter-volume aqueous droplets in microfluidic systems, Appl. Phys. Lett. **87**, 031916 (2005).

[20] M. He, J. S. Kuo, and D. T. Chiu, Effects of ultrasmall orifices on the electrogeneration of femtoliter-volume aqueous droplets, Langmuir **22**, 6408 (2006).

[21] M. Shojaeian, F.-X. Lehr, H. U. Göringer, and S. Hardt, On-demand production of femtoliter drops in microchannels and their use as biological reaction compartments, Anal. Chem. **91**, 3484 (2019).

[22] See the supplemental material at http://link.aps.org/supplemental/10.1103/PhysRevApplied.13.014015 for Video 1, showing a droplet reciprocating between two liquid interfaces.

[23] J. C. Bird, W. D. Ristenpart, A. Belmonte, and H. A. Stone, Critical Angle for Electrically Driven Coalescence of two Conical Droplets, Phys. Rev. Lett. **103**, 1 (2009).

[24] C. T. Bartlett, G. A. Généro, and J. C. Bird, Coalescence and break-up of nearly inviscid conical droplets, J. Fluid Mech. **763**, 369 (2015).

[25] L. G. Leal, *Advanced Transport Phenomena* (Cambridge University Press, Cambridge, 2007).

[26] H. M. Sadeghi, B. Sadri, M. A. Kazemi, and M. Jafari, Coalescence of charged droplets in outer fluids, J. Colloid Interface Sci. **532**, 363 (2018).

[27] K. Sainath and P. Ghosh, Stabilization of silicone oil-in-water emulsions by ionic surfactant and electrolytes: The role of adsorption and electric charge at the interface, Ind. Eng. Chem. Res. **52**, 15808 (2013).

[28] F. Lacharme and M. A. M. Gijs, Single potential electrophoresis microchip with reduced bias using pressure pulse injection, Electrophoresis **27**, 2924 (2006).

[29] P. H. Chiu, C. C. Chang, and R. J. Yang, Electrokinetic micromixing of charged and non-charged samples near nano-microchannel junction, Microfluid. Nanofluid. **14**, 839 (2013).

[30] A. H. A. Razak and A. L. Skov, Silicone elastomers with covalently incorporated aromatic voltage stabilisers, RSC Adv. **7**, 468 (2017).